Interaction-induced analog of a non-Hermitian skin effect in a lattice two-body problem

Alexander N. Poddubny ●[*]

Rehovot 761001, Israel

We present a theoretical study of the quantum states of two repelling spinless particles in a one-dimensional tight-binding model with a simple periodic lattice and open boundary conditions. We demonstrate that, when the particles are not identical, their interaction drives nontrivial correlated two-particle states, such as bound states and edge states, and induces interaction-induced flat bands. We show that the localization of the center of mass of the two particles enforces the localization of their relative motion, which means formation of the bound states. While the considered system is Hermitian, an insight into the bound states is provided by an approximate effective non-Hermitian model for the relative motion that features the non-Hermitian skin effect.

I. INTRODUCTION

In recent decades, topology-inspired ideas have become a universal framework to characterize various natural phenomena. First, topological excitations, solitons, and vortices were found in various systems with nonlinearity and interactions [1]. Next, it was understood that even noninteracting periodic systems, described by linear equations, can be assigned quantized topological indices, and localized excitations arise at the boundaries where such indices exhibit an abrupt change [2,3]. Such localized excitations, topological edge states, can form from different species of particles, from electrons to photons to mechanical vibrations [4]. Even more recently, self-induced edge states with nontrivial topology assisted by nonlinearity became a subject of active studies [5–8]. Another aspect of the interplay of topology and interactions that involves not only the edge states but also the bound states, has been put forward in Refs. [9,10]. It has been understood that topological nontrivial Hamiltonians may be realized in the systems of several interacting particles even without any physical boundaries. In this case, one of the particles can provide a boundary that traps another particle, thus forming a bound state. This localization mechanism has a certain similarity with the one discussed in Refs. [6,11]; however, it also involves the so-called non-Hermitian skin effect [12–17], which means localization of the bulk eigenstates in the non-Hermitian system. As a result, the relative motion of the two particles with respect to each other becomes restricted. One could term such kind of states as "topologically bound," in contrast to usual topological edge states. These bound states are related to the topology of the complex spectrum of non-Hermitian systems [18,19], rather than the topology of the wave functions which is behind the edge states in topological insulators and superconductors [2,20]. Importantly, the bound states considered in Refs. [9,10,21,22] also required the non-reciprocity and/or non-Hermiticity of the system even in the absence of interaction.

Here, we show that topologically bound states and a series of interaction-induced flat bands can be realized in an even simpler situation of two distinguishable interacting particles of different masses under open boundary conditions. At the single-particle level the model is reciprocal and Hermitian, while contact repulsion drives complex two-particle correlations and localizations. All these two-particle correlations are just a consequence of the different masses of the two particles. While localization of light particles on the heavy ones has been analyzed in literature [23–26], here we show that the resulting bound states can be interpreted as a result of the non-Hermitian skin effect arising for the relative motion in the presence of interactions. Contrary to Refs. [27,28], the non-Hermiticity is not explicitly built in the model at the single-particle level and contrary to Ref. [29], that studied the breakdown of Hermiticity due to the specially engineered nonlocal quantum nonlinearity, we consider only the local interaction term. The effective non-Hermiticity arises in our problem only from the simplified description for the relative motion of interacting particles in the reference frame where their center of mass is localized. Hence, our results provide a mechanism how the topologically nontrivial effect, usually considered for non-Hermitian systems, can arise also in the interacting Hermitian system. Since considered correlated states do not require any special lattice engineering, as in a Su-Schrieffer-Heeger (SSH) model [7,30,31], or even unusual long-ranged couplings as in the case of waveguide-coupled atom arrays [6,32], they should be readily observable. A suitable platform could be lattices of trapped cold atoms, where bound states of two interacting identical particles have been observed [33]. Notably, the two-particle model with different masses has been considered before in detail [34–36]. In Ref. [36] even the formation of a single flat band has been predicted for the structure with an impurity. Here, however, instead of the impurity we consider open boundary conditions. Moreover, we obtain a series of flat bands with different energies instead of a single flat band.

The rest of the paper is organized as follows. Section II presents the model and outlines our main results. Section III contains the qualitative analytical argument for the formation
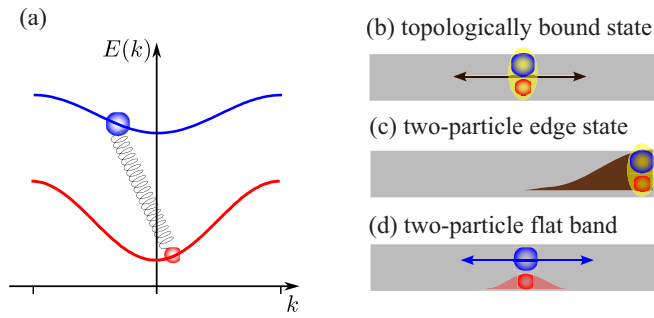
---

*alexander.poddubnyy@weizmann.ac.il

FIG. 1. (a) Schematics of the energy dispersion branches $E(k)$ for two distinguishable particles in a one-dimensional lattice. (b)–(d) Correlated states arising from a two-particle interaction: (b) *topologically bound* state of two particles, (c) two-particle edge state, and (d) two-particle flat-band state, where one of the particles is localized and the other one is delocalized.

of the topologically bound state in this model. Next, in Sec. IV, we discuss the calculated eigenstates of the two-particle Schrödinger equation. Section V details the origin of interaction-induced flat bands in our system and some details are reserved for Appendix.

II. MODEL

We consider a paradigmatic one-dimensional (1D) tight-binding model of two different spinless particles 1 and 2, that exhibit a contact repulsion, as described by the Hamiltonian

$$H = \sum_{\nu=1,2} \left[\sum_{n=1}^{N} \varepsilon_\nu b_n^{(\nu)\dagger} b_n^{(\nu)} + \sum_{n=1}^{N-1} \left[t_\nu b_n^{(\nu)\dagger} b_{n+1}^{(\nu)} + \text{H.c.} \right] \right]$$
$$+ U \sum_{n=1}^{N} \left(b_n^{(1)\dagger} b_n^{(1)} \right) \left(b_n^{(2)\dagger} b_n^{(2)} \right). \quad (1)$$

Each of the particles is characterized by a site energy $\varepsilon_{1,2}$ and a tunneling constant $t_{1,2}$, that yield the dispersion laws $\varepsilon_\nu(k) = \varepsilon_\nu + 2t_\nu \cos k$ in the absence of the interactions (k is the quasimomentum). The two corresponding dispersion curves are schematically shown in Fig. 1(a). Their curvatures (particle masses) differ since $t_1 \neq t_2$. Here, the operators $b^{(1,2)\dagger}$ describe the creation of the particles in bands 1 and 2. Since the considered problem has exactly one particle in each of the bands, and these two particles are distinguishable, $[b^{(1)\dagger}, b^{(2)\dagger}] = 0$, it is not important for the studied problem whether the particle statistics is bosonic or fermionic.

Our goal is to examine the role of the interaction term [the last line in Eq. (1)] on the two-particle correlations in the strong interaction regime when $|U| \gg |t_{1,2}|$. Namely, we demonstrate that for a finite number of sites N this model has quite a rich structure of two-particle eigenstates $|\Psi\rangle \equiv \sum_{nm} \psi_{nm} b_n^{(1)\dagger} b_m^{(2)\dagger} |0\rangle$, including bound states [Fig. 1(b)], two-particle edge states [Fig. 1(c)], and also unusual two-particle correlated states where one of the particles is localized and the second one is not [Fig. 1(d)]. We show that such two-particle states are degenerate with respect to the heavier particle position and form a series of flat bands [37].
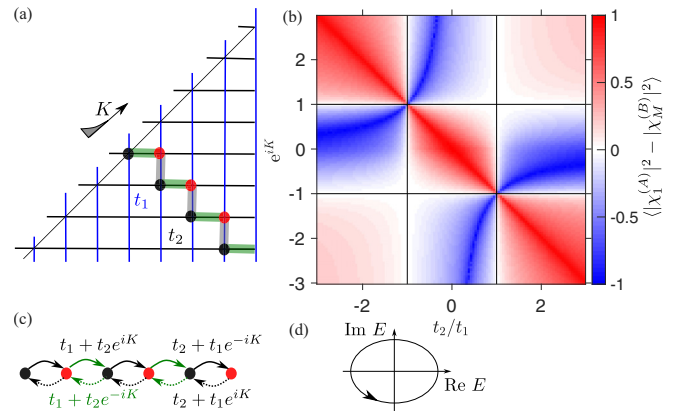

FIG. 2. (a) Scheme of the interaction of two particles with the center-of-mass wave vector K. (b) Interaction-induced Su-Schrieffer-Heeger model with the couplings indicated above the arrows. (c) Localization parameter $|\chi_1^{(A)}|^2 - |\chi_M^{(B)}|^2$ depending on the ratio of the tunneling constants t_2/t_1 and on the center-of-mass wave vector K. (d) Winding of the complex energies, Eq. (3), in the bulk around the coordinate origin.

III. TOPOLOGICALLY BOUND STATES

We start the analysis by writing the two-particle Schrödinger equation for the wave function $\psi_{nm} = \chi_{n-m} \exp[iK(n+m)]$, where K is the center-of-mass wave vector and the amplitude χ characterizes the relative motion. For simplicity we always consider a situation where the order of particles is fixed, that is, either $n > m$ or $n < m$. This can be viewed as a two-particle version of the Bethe ansatz. The interacting two-particle model is then formally equivalent to the single-particle model on the right-angular discrete billiard in two dimensions (2D), as shown in Fig. 2(a). Such discrete billiard was recently analyzed in detail in Ref. [38], but neither bound nor localized states were considered there. Vertical and horizontal motion in the 2D lattice correspond to the motion of the first and second particle, respectively. In the relative reference frame such model corresponds to a zigzag chain with two sites per unit cell, that we will label A and B [thick line in Fig. 2(a)]. The Schrödinger equation for the amplitude χ_n assumes the form

$$\varepsilon \chi_n^{(A)} = (t_2 + t_1/z)\chi_n^{(B)} + (t_1 + t_2/z)\chi_{n-1}^{(B)},$$
$$\varepsilon \chi_n^{(B)} = (t_2 + t_1 z)\chi_n^{(A)} + (t_1 + t_2 z)\chi_{n+1}^{(A)}, \quad (2)$$

where $z = e^{iK}$ and $n = 1, 2, \ldots$. As soon as the wave-function amplitude, describing the center of mass motion, exponentially decays in space (i.e., $\text{Im } K \neq 0$), the system, Eq. (2), realizes a non-Hermitian Su-Schrieffer-Heeger model [18,19], illustrated in Fig. 2(b). Such model features the non-Hermitian skin effect [12,13,16,17]: all its eigenstates can become localized at the edge. This feature is specific for a non-Hermitian system and it is related to the nontrivial winding number of the eigenvalues of Eq. (2) in the bulk for a periodic solution of the form $\chi_n \propto e^{i\kappa n}$, where κ is the eigenvector [39–41]. The complex eigenenergy is given by

$$E(\kappa) = \pm \sqrt{t_2 + t_1/z + (t_1 + t_2/z)e^{-i\kappa}}$$
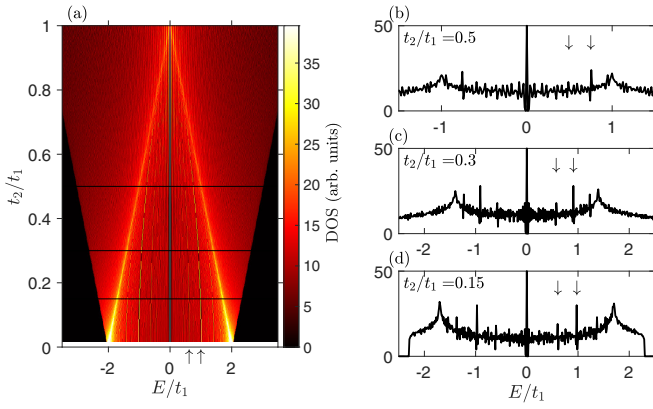$$\times \sqrt{t_2 + t_1 z + (t_1 + t_2 z)e^{i\kappa}}. \quad (3)$$

FIG. 3. (a) Density of states depending on the value of the tunneling constants t_2/t_1 for $N = 101$. (b)–(d) Cross sections of (a) for three different values of t_2/t_1, indicated on graphs and also shown by horizontal lines in (a).

It can be directly checked that for $z \neq 1$, $t_2 \neq t_1$, Eq. (3) winds once around the point $E = 0$ as κ changes from $-\pi$ to π, as shown in Fig. 2(d). In order to see how the eigenstates become localized one can, e.g., substitute $\chi_n^{(B)} = 0$ into the second of Eq. (2) and find

$$\chi_n^{(A)} \propto \left(\frac{t_1 z + t_2}{t_2 z + t_1} \right)^n. \tag{4}$$

Thus, as soon as $|t_1| \neq |t_2|$ and $|z| \neq 1$, the states become localized which turns out to be a generic topological feature. In order to better illustrate this we have plotted numerically the localization parameter $|\chi_1^{(A)}|^2 - |\chi_M^{(B)}|^2$, averaged over all the eigenstates, for a finite number of unit cells $n = 1, \ldots, M = 20$ depending on the ratio t_1/t_2 and on the center-of-mass parameter z. The calculation demonstrates the formation of localized states either at the left edges (red shading) or at the right edges (blue shading), in agreement with Eq. (2). While the calculations here and below correspond to the limit of infinitely strong interaction U, the results remain qualitatively the same for finite but large $|U| \gg |t_{1,2}|$.

Our analysis thus predicts that for different masses of two strongly interacting particles their center-of-mass motion, described by K, and their relative motion, described by χ, are not independent but rather coupled in a topologically nontrivial way. By virtue of the non-Hermitian effect the localization of the center of mass enforces constraints on the relative motion, i.e., formation of the bound states. Next, we will show by a rigorous numerical calculation of the two-particle eigenstates that the center of mass can be localized indeed in a finite 1D array and that the bound states form.

IV. TWO-PARTICLE EIGENSTATES

We present the two-particle state as $\Psi = \sum_{n=1}^{N} \sum_{m=n+1}^{N} \psi_{nm} b_n^{(1)\dagger} b_m^{(2)\dagger} |0\rangle$, and solve numerically the Schrödinger equation $H\Psi = E\Psi$ with the Hamiltonian equation (1) for the two-particle amplitudes ψ_{nm} in the limit $U \to \infty$. We use $\varepsilon_1 + \varepsilon_2$ as a reference point for the energy, which is equivalent to setting $\varepsilon_{1,2} = 0$. Figure 3 presents the density of states (DOS) numerically calculated for varying
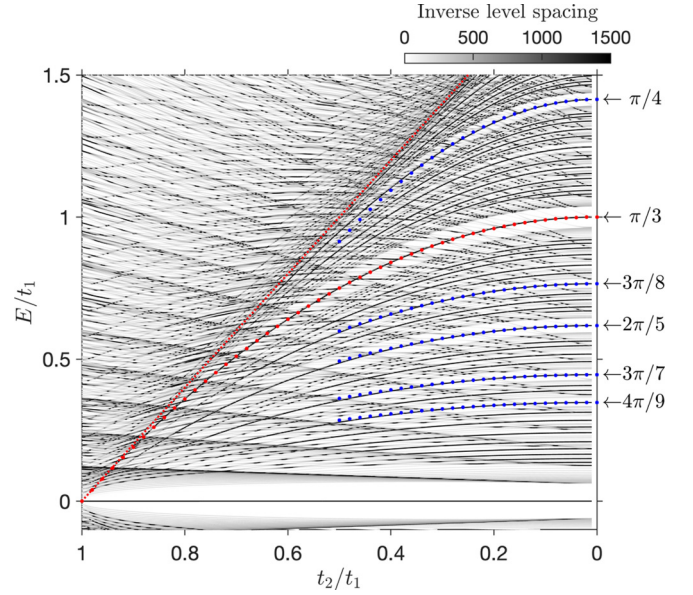

FIG. 4. Energy of the two-particle states depending on the value of the tunneling constants t_2/t_1 calculated for $N = 101$ and $t_1 = 1$. The intensity of grayscale shading corresponds to the inverse spacing between neighboring levels. Dotted line shows the dependence $E = 2(t_1 - t_2)$. Horizontal arrows indicate the energies $E = 2t_1 \cos k$, with the values of k given near each arrow. Dotted parabolas show the energies of the corresponding states calculated up to the second order in t_2.

ratio t_2/t_1. This ratio of the two tunneling constants t_2/t_1 turns out to be the key parameter of the model. Panel (a) shows the DOS as a color map, and panels (b)–(d) show the plots of the DOS vs the energy E for three characteristic ratios of t_2/t_1. Importantly, the DOS is a strongly nonmonotonous function of energy. First, it features van Hove singularities at the energies $E = \pm 2(t_1 - t_2)$, corresponding to the extrema of single-particle dispersions $2t_{1,2} \cos k$. These singularities manifest themselves as sharp maxima that are best seen for $t_2 = 0$, when they are located at $E = \pm 2t_1$ [see the bottom of Figs. 3(a) and 3(d)]. However, there also exist additional sharp peaks in the DOS, not associated with the van Hove singularities. These extra sharp peaks are indicated by two vertical arrows in each of the panels of Fig. 3. They correspond to the almost-degenerate states and arise from the interplay of the discreteness of the system and the interactions. The presence of such peaks can be also seen in Fig. 4 where we show the same energy levels separately. In order to highlight the presence of degenerate states, corresponding to the interaction-induced flat bands, the intensity of the grayscale shading represents the inverse level spacing. In such way the degenerate states become brighter and stand out. Several sets of such states are highlighted by the dotted parabolas, that correspond to the DOS peaks discussed above. The two arrows in Fig. 3 correspond to the parabolas labeled as $\pi/3$ and $2\pi/5$ in Fig. 4. The origin of such notation will be discussed in Sec. V. The eigenstates ψ_{nm} at these DOS peaks feature unusual two-particle correlations.

Figure 5 examines in detail the spatial profile of the eigenstates for $t_2/t_1 = 0.4$ (a), (b) and $t_2/t_1 = 0.8$ (c), (d). The left
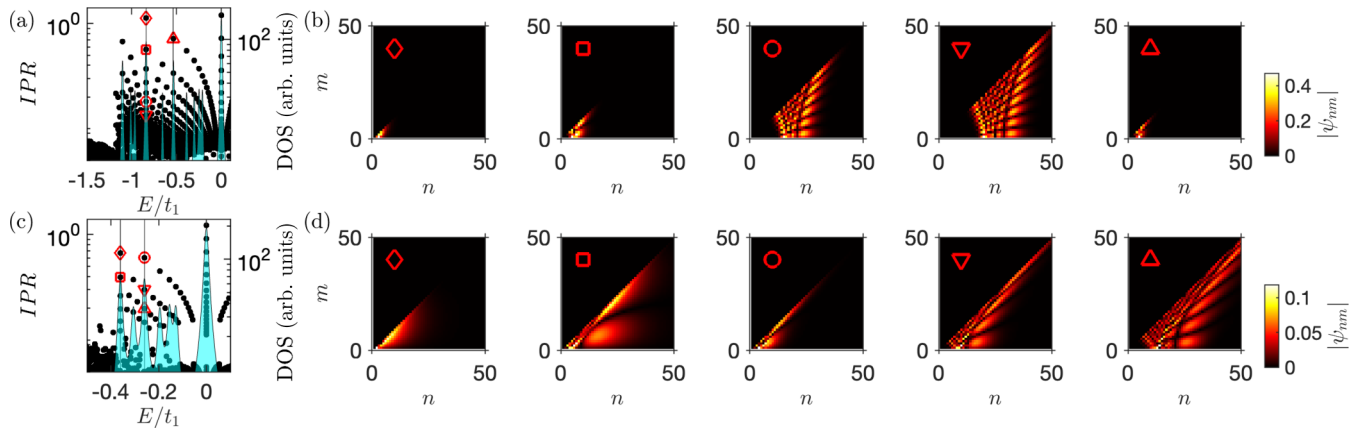
FIG. 5. (a), (c) Energies of two-particle states vs inverse participation ratio (IPR) calculated for $t_2/t_1 = 0.4$ (a) and $t_2/t_1 = 0.8$ (c). Open symbols indicate specific eigenstates, with the corresponding wave functions shown in (b) and (d). Right y axis shows by the blue-shaded curves the density of states for all the states with the IPR larger than 0.3.

panels (a) and (c) present the inverse participation ratio (IPR), which is defined as $\sum_{nm} |\psi_{nm}|^4 / (\sum_{nm} |\psi_{nm}|^2)^2$ depending on the eigenstate energy. The larger the IPR the stronger the eigenstate localization. The calculation shows that most of the eigenstates are spatially extended, that is, they have an IPR much smaller than unity. However, there exist also groups of almost degenerate states with high IPR. They correspond to the points in Figs. 5(a) and 5(c) lying on the same vertical lines. The same is evidenced by the density of states peaks, shown in Figs. 5(a) and 5(c) by the curves with blue shading, corresponding to the right abscissa axis. The two vertical lines in Fig. 5 indicate the same peaks in the density of states that are denoted by the arrows in Fig. 3. We also note the presence of a large central peak at $E = 0$. This peak is associated with the chiral symmetry of the problem and corresponds to the states with a checkerboard profile, localized on only part of the sites of the square lattice, that is, $\psi_{nm} \neq 0$ when n and m have different parity [38]. If only nearest-neighbor couplings are included, all these states are exactly degenerate. Since they form a large degenerate subspace, their spatial profile is not well defined. Depending on what linear combination is chosen, one can obtain strongly localized states with a large IPR, as can be seen in Figs. 5(a) and 5(c). In our numerical calculation, we have added a small additional second nearest-neighbor coupling of 0.0002 for the first particle. This does not significantly affect the state energy but fixes the gauge for degenerate states. In this work, however, we are interested in the states with $E \neq 0$, that are gauge independent.

The panels in Figs. 5(b) and 5(d) show the spatial profiles $|\psi_{nm}|^2$ for several characteristic two-particle states, indicated by symbols in Figs. 5(a) and 5(c). The abscissa and ordinate on these plots correspond to the coordinates of the two particles. Crucially, the spatial distribution of the two-particle correlations is highly inhomogeneous. For example, the first two states in Fig. 5(b) (diamond and square symbols), correspond to both particles localized at the edge of the lattice. This is a two-particle edge state, akin to Fig. 1(c). The next two states (circle and down-pointing triangle) realize the situation when one particle is relatively localized and the other one is spread over the whole lattice. This is the state in Fig. 1(d). There exist many such states that differ only by a position

of the localized particle. Since they are degenerate, they can be seen as an interaction-induced flat band. The last state in Fig. 5(b) (upward-pointing triangle) is also a two-particle edge state, but with a different energy.

As the ratio of the tunneling constants increases to $t_2/t_1 = 0.8$, the eigenstates become generally less localized in space, as can be seen in the overall increase of the IPR in Fig. 5(c) as compared to Fig. 5(a). This is expected, since the origin of localization is the difference of the particle masses. A less expected effect is that the relative motion of the particles for larger t_2/t_1 also becomes constrained. Namely, the first three states in Fig. 5(c) (diamond, square, and circle symbols) can be interpreted as the two-particle bound states, localized at the edge. The last two states (triangles) are of somewhat intermediate character. They resemble both the above-mentioned state where only one of the particles is localized and also the two-particle bound state.

Thus, our rigorous numerical calculations confirm the formation of two-particle bound states, localized at the structure edge, in agreement with the non-Hermitian SSH model in Fig. 2(b). In order to further support the connection of the formation of a bound state with the non-Hermitian skin effect we analyze in Fig. 6 in more detail the eigenstate in Fig. 5(d), indicated by a circle. In the main part of Fig. 6 we present the cuts of the distribution $|\psi_{nm}|^2$ along the direction corresponding to the relative motion of the two particles. The specific points used for the cuts are indicated by the zigzag lines in the inset, that also shows the same spatial distribution $|\psi_{nm}|^2$. All of the cuts decay with the distance which reflects the confinement of the two particles to each other. The difference between the cuts corresponds to the localization of the center of mass at the edge of the structure. Fitting this decay we were able to extract the center-of-mass localization parameter $z \equiv \exp(iK) \approx -0.85$ for this eigenstate. Next, we have used this parameter in the effective non-Hermitian SSH model, Eq. (2). The resulting distribution of the eigenstate of the effective model with the closest energy is shown in Fig. 6 by open circles. This state decays in space and the scale of the decay satisfactorily reproduces the results of full numerical calculation (filled symbols). This agreement supports our interpretation of the formation of the bound state
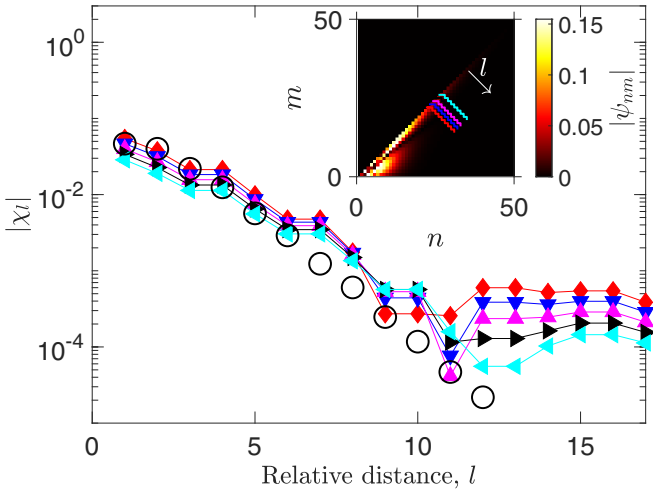
FIG. 6. Two-particle wave function of the "topologically bound" state depending on the distance l between the two particles. Filled triangles with different orientation correspond to the different center-of-mass coordinates $n = 22 \ldots 26$. The points have been obtained by cutting the total wave function $|\psi_{mn}|$ in the direction of the relative motion along the colored zigzag lines, shown in the inset. Open circles correspond to the eigenstate of the system, Eq. (2), calculated for $z \equiv \exp(iK) = -0.85$ for the most localized state with $E \approx -0.259t_1$, which is indicated by a circle in Figs. 5(c) and 5(d). Other calculation parameters are $t_2/t_1 = 0.8$ and $N = 101$.

as a result of a non-Hermitian skin effect for the relative motion.

The fact that such bound states arise only for relatively high values of t_2/t_1, close to unity, also well agrees with the non-Hermitian SSH model. It is clearly seen in Fig. 2(c) that the darker color, which means stronger localization, corresponds to the regions with t_2/t_1 close to unity.

The analysis above leaves two more open questions. First, what is the specific origin of the center-of-mass localization at the edge? Second, how and why form the flat bands, i.e., almost degenerate eigenstates? These questions turn out to be related and will be addressed in the next section.

V. INTERACTION-INDUCED WANNIER-STARK LADDER

The formation of degenerate and localized states can be most easily understood in the limit when $t_2 \ll t_1$, that is, when one of the two particles is much heavier than the other one. In this case the motion of the heavier particle can be considered as a perturbation. This means that the triangular lattice in Fig. 2 separates into vertical columns of varying height (blue color). One can first find the eigenstates within each column and then describe the coupling between the columns $\propto t_2$. The column height variation imposes an additional potential, that depends on the column height. Such model with coupled columns is in fact very similar to the tight-binding model for the particle on a 1D lattice in a constant electric field, that is described by a Wannier-Stark ladder [42–44]. We stress that the considered Stark-like localization is quite distinct from the many-body Stark localization studied in Refs. [45,46], since there is no external electric field in the system. The effective electric field appears only because of the interactions.

In order to formally derive the model with coupled columns we start by writing the Schrödinger equation in a tight-binding model for every column, that is,

$$t_1(\psi_{m-1,n} + \psi_{m+1,n}) = \varepsilon \psi_{m,n} \tag{5}$$

with the open boundary conditions, $m = 1, \ldots, n-1$. Its eigenstates are the usual standing waves

$$\psi_{mn}^{(\nu)} \approx \sqrt{\frac{2}{n-1}} \sin k_n^{(\nu)} m, \text{ where } k_x^{(j)} = \frac{\pi j}{n}, \tag{6}$$

$m, \nu = 1, 2, \ldots, n-1$, with the energies

$$\varepsilon_n^{(\nu)} = 2t_1 \cos k_n^{(\nu)}. \tag{7}$$

Importantly, for each $n = 3, 6, \ldots$, that is divisible by 3, there exists an eigenstate with an integer $\nu = n/3$, so that $\cos k_n^{(\nu)} = 1/2$ and $\varepsilon_n^{(\nu)} = t_1$. We now take into account the coupling between the states, Eq. (6), i.e., the interaction between the "columns" that is proportional to the tunneling constant t_2:

$$\langle \nu, n | \nu', n+1 \rangle \equiv t_2 \sum_{m=1}^{n-1} \psi_{m,n}^{(\nu)} \psi_{m,n+1}^{(\nu')}$$

$$= -t_2 \frac{1}{\sqrt{n(n-1)}} \frac{\sin k_n^{(\nu)} \sin k_{n+1}^{(\nu')}}{\cos k_n^{(\nu)} - \cos k_{n+1}^{(\nu')}}. \tag{8}$$

We can now formally write the system of equations describing coupled columns

$$\varepsilon_n^{(\nu)} \psi_n^{(\nu)} + \langle \nu, n | \nu', n+1 \rangle \psi_{n+1}^{(\nu)} + \langle \nu, n | \nu', n-1 \rangle \psi_{n-1}^{(\nu)}$$
$$= \varepsilon_n^{(\nu)} \psi_n^{(\nu)}. \tag{9}$$

This is equivalent to rewriting the original two-particle Schrödinger equation into the standing-wave basis only for one of the particles.

We now assume that $\nu = n_0/3$ with an integer $n_0 \gg 1$ and take into account only one standing wave ν. Next, we expand the matrix element, Eq. (8), in the limit where $k^{(\nu)} \approx \pi/3$. This results in the following equation:

$$[F(n - n_0) + \alpha(n - n_0)^2]\psi_n + \tau(\psi_{n+1} + \psi_{n-1}) = \varepsilon \psi_n, \tag{10}$$

with the rescaled energy $\varepsilon = E/t_1 - 1$, the parameter $F = \pi/\sqrt{3}n_0$ being the dimensionless electric field, $\alpha = -\pi(6\sqrt{3} + \pi)/18n_0^2$ and $\tau = 3\sqrt{3}t_2/(2\pi t_1)$. The index ν is dropped for simplicity. Contrary to the original Wannier-Stark model, here we also take into account the quadratic correction to the potential $\propto \alpha$. As shown in the Appendix, for $|\alpha| \ll |F|$ the system, Eq. (10), has an eigenvalue

$$\varepsilon = -2\alpha \frac{\tau^2}{F^2} \approx -0.98 \left(\frac{t_2}{t_1}\right)^2 = \text{const}(n_0), \tag{11}$$

corresponding to the state of the Wannier-Stark ladder localized at the site $n = n_0$. We stress that the eigenenergy, Eq. (11), does not depend on the column height n_0. This means the formation of a set of degenerate states differing by the value of n_0. These are exactly the states in Fig. 5(b) shown by the diamond, square, circle, and down-pointing triangle. Their energies are given by $|E| = t_1 - t_2^2/t_1$, in agreement

with Eq. (11). This expression is plotted by the parabola with big red dots in Fig. 4 and perfectly agrees with the result of exact numerical calculation.

A similar analysis can be made for the other DOS peaks. We show several values of $k^{(\nu)}$, namely, $k^{(\nu)} = \pi/4, 3\pi/8, 2\pi/5, 3\pi/7, 4\pi/9$, and the corresponding energies $2t_1 \cos k^{(\nu)}$ by the horizontal arrows in Fig. 4. This Wannier-Stark-like model describes both localization and degeneracy of the spectrum in the limit when $t_2 \ll t_1$. At small values of t_2 the dependence of the energies on $t^{(2)}$ is parabolic and can be calculated by the perturbation series, $E(t_2) = E(t_2 = 0) - \nu t_2^2/t_1$. The corresponding expressions are plotted in Fig. 4 as dotted parabolas, with the coefficient $\nu = 2, 1, 2/3, 1/2, 1/3, 1/4$ corresponding to the parabolas from top to bottom. For larger value of t_2 the coupling constant τ increases and the localization becomes weaker, but still survives. At the same time, due to the coupling between center of mass and relative degrees of freedom, the two particles become bound to each other as discussed in Sec. III. This can be seen from a comparison of the states shown by diamonds and squares in Figs. 5(b) and 5(d). Our numerical analysis thus indicates that with the increase of t_2/t_1 there occurs a transformation from the states where a light particle is localized on the immobile heavy one to the two-particle bound states, localized as a whole at the edge of the structure.

Our consideration has been focused on the simplest tight-binding model with only nearest-neighbor couplings. Numerical calculation shows that all the types of eigenstates shown in Fig. 5, including the "topologically bound" states, survive also if longer-ranged couplings are included provided that these couplings are weaker than the nearest-neighbor couplings. The results are generally more sensitive to the couplings between second or other even-numbered nearest neighbors that break the chiral symmetry of the problem. The spectrum loses mirror symmetry around the point $\varepsilon = 0$ and the flat-band degeneracy is broken. Couplings between the neighbors with an odd distance (first, third, etc.), keep the chiral symmetry. While they also break the flat-band degeneracy, their overall effect on the spectrum and eigenstates is weaker.

VI. SUMMARY AND OUTLOOK

To summarize, we have considered a discrete two-particle problem in a one-dimensional tight-binding model without any non-Hermiticity at the single-particle level. We have demonstrated that when the particles are not identical, complex correlated states can result from their interaction, that can be linked to a non-Hermitian topological physics. It remains to be understood what happens in the many-body case and in more complicated lattices.

APPENDIX: PERTURBATION THEORY

Here we analyze in more detail the Wannier-Stark-like model, Eq. (10), in the limit where $|\alpha| \ll 1$. We first start from the simpler case where also $|\tau| \ll 1$. The energy of the eigenstate that is localized at the site $n = n_0$, can be then found by a simple second-order perturbation theory in τ, accounting for the coupling of this site to its two neighbors:

$$\varepsilon \approx \frac{\tau^2}{F - \alpha} + \frac{\tau^2}{F + \alpha} \approx \frac{2\alpha\tau^2}{F^2}. \quad (A1)$$

Since α/F^2 does not depend on the number of the point n_0, where the first particle is localized, the states for different points n_0 are degenerate.

The interesting finding is that the answer, Eq. (A1), remains valid even if $\tau \sim 1$, provided that still $|\alpha| \ll 1$. To prove this we account for the term $\alpha(n - n_0)^2$ in Eq. (10) by a first-order perturbation theory in α. For $\alpha = 0$ Eq. (10) have eigenstates

$$\psi_n = J_n(-2\tau/F). \quad (A2)$$

The first-order perturbation theory correction is given by

$$\alpha \sum_{n=-\infty}^{\infty} |J_n(-2\tau/F)|^2 n^2. \quad (A3)$$

We will now show that this sum is exactly equal to Eq. (A1) for an arbitrary value of τ/F. For this we explicitly use the fact that Eq. (A2) is an eigenstate of Eq. (10) for $\alpha = 0$. This means that

$$\alpha n^2 J_n^2(-2\tau/F) = \frac{\alpha\tau^2}{F^2}[J_{n-1}(-2\tau/F) + J_{n+1}(-2\tau/F)]^2$$
$$= \frac{\tau^2}{F^2}[J_{n-1}^2(-2\tau/F) + J_{n+1}^2(-2\tau/F)$$
$$+ 2J_{n-1}(-2\tau/F)J_{n+1}(-2\tau/F)]. \quad (A4)$$

The summation over n can be now performed analytically. The first two terms in the square brackets in the right-hand side yield unity because of the normalization condition $\sum_n J_n^2(-2\tau/F) = 1$. The last term is zero because $J_{n+1}(-2\tau/F)$ and $J_{n-1}(-2\tau/F)$ are two different eigenstates of the Wannier-Stark problem, Eq. (10), with $\alpha = 0$, hence they are orthogonal to each other. This leads to the result, Eq. (A1).

[1] N. Manton and P. Sutcliffe, *Topological Solitons* (Cambridge University Press, Cambridge, UK, 2004).

[2] M. Z. Hasan and C. L. Kane, *Colloquium*: Topological insulators, Rev. Mod. Phys. **82**, 3045 (2010).

[3] T. Ozawa, H. M. Price, A. Amo, N. Goldman, M. Hafezi, L. Lu, M. C. Rechtsman, D. Schuster, J. Simon, O. Zilberberg, and I. Carusotto, Topological photonics, Rev. Mod. Phys. **91**, 015006 (2019).

[4] G. Ma, M. Xiao, and C. T. Chan, Topological phases in acoustic and mechanical systems, Nat. Rev. Phys. **1**, 281 (2019).

[5] A. N. Poddubny and D. A. Smirnova, Ring Dirac solitons in nonlinear topological systems, Phys. Rev. A **98**, 013827 (2018).

[6] A. V. Poshakinskiy, J. Zhong, Y. Ke, N. A. Olekhno, C. Lee, Y. S. Kivshar, and A. N. Poddubny, Quantum Hall phases emerging from atom–photon interactions, npj Quantum Inf. **7**, 34 (2021).

[7] N. A. Olekhno, E. I. Kretov, A. A. Stepanenko, P. A. Ivanova, V. V. Yaroshenko, E. M. Puhtina, D. S. Filonov, B. Cappello, L. Matekovits, and M. A. Gorlach, Topological edge states of interacting photon pairs emulated in a topolectrical circuit, Nat. Commun. **11**, 1436 (2020).

[8] M. S. Kirsch, Y. Zhang, M. Kremer, L. J. Maczewsky, S. K. Ivanov, Y. V. Kartashov, L. Torner, D. Bauer, A. Szameit, and M. Heinrich, Nonlinear second-order photonic topological insulators, Nat. Phys. **17**, 995 (2021).

[9] C. H. Lee, Many-body topological and skin states without open boundaries, Phys. Rev. B **104**, 195102 (2021).

[10] R. Shen and C. H. Lee, Non-Hermitian skin clusters from strong interactions, Commun. Phys. **5**, 238 (2022).

[11] J. Zhong, N. A. Olekhno, Y. Ke, A. V. Poshakinskiy, C. Lee, Y. S. Kivshar, and A. N. Poddubny, Photon-Mediated Localization in Two-Level Qubit Arrays, Phys. Rev. Lett. **124**, 093604 (2020).

[12] T. E. Lee, Anomalous Edge State in a Non-Hermitian Lattice, Phys. Rev. Lett. **116**, 133903 (2016).

[13] V. M. Martinez Alvarez, J. E. Barrios Vargas, and L. E. F. Foa Torres, Non-Hermitian robust edge states in one dimension: Anomalous localization and eigenspace condensation at exceptional points, Phys. Rev. B **97**, 121401(R) (2018).

[14] F. K. Kunst, E. Edvardsson, J. C. Budich, and E. J. Bergholtz, Biorthogonal Bulk-Boundary Correspondence in Non-Hermitian Systems, Phys. Rev. Lett. **121**, 026808 (2018).

[15] S. Yao and Z. Wang, Edge States and Topological Invariants of Non-Hermitian Systems, Phys. Rev. Lett. **121**, 086803 (2018).

[16] D. S. Borgnia, A. J. Kruchkov, and R.-J. Slager, Non-Hermitian Boundary Modes and Topology, Phys. Rev. Lett. **124**, 056802 (2020).

[17] N. Okuma, K. Kawabata, K. Shiozaki, and M. Sato, Topological Origin of Non-Hermitian Skin Effects, Phys. Rev. Lett. **124**, 086801 (2020).

[18] E. J. Bergholtz, J. C. Budich, and F. K. Kunst, Exceptional topology of non-Hermitian systems, Rev. Mod. Phys. **93**, 015005 (2021).

[19] N. Okuma and M. Sato, Non-Hermitian topological phenomena: A review, arXiv:2205.10379.

[20] C.-K. Chiu, J. C. Y. Teo, A. P. Schnyder, and S. Ryu, Classification of topological quantum matter with symmetries, Rev. Mod. Phys. **88**, 035005 (2016).

[21] F. Qin, R. Shen, and C. H. Lee, Non-Hermitian squeezed polarons, arXiv:2202.10481.

[22] J. M. Koh, T. Tai, and C. H. Lee, Simulation of Interaction-Induced Chiral Topological Dynamics on a Digital Quantum Computer, Phys. Rev. Lett. **129**, 140502 (2022).

[23] Y. Kagan and L. Maksimov, Localization in a system of interacting particles diffusing in a regular crystal, Sov. Phys. JETP **60**, 201 (1984).

[24] T. Grover and M. P. A. Fisher, Quantum disentangled liquids, J. Stat. Mech. (2014), P10010.

[25] W. De Roeck and F. Huveneers, Scenario for delocalization in translation-invariant systems, Phys. Rev. B **90**, 165137 (2014).

[26] N. Y. Yao, C. R. Laumann, J. I. Cirac, M. D. Lukin, and J. E. Moore, Quasi-Many-Body Localization in Translation-Invariant Systems, Phys. Rev. Lett. **117**, 240601 (2016).

[27] S.-B. Zhang, M. M. Denner, T. Bzdušek, M. A. Sentef, and T. Neupert, Symmetry breaking and spectral structure of the interacting Hatano-Nelson model, Phys. Rev. B **106**, L121102 (2022).

[28] K. Kawabata, K. Shiozaki, and S. Ryu, Many-body topology of non-Hermitian systems, Phys. Rev. B **105**, 165137 (2022).

[29] W. N. Faugno and T. Ozawa, Interaction-Induced Non-Hermitian Topological Phases from a Dynamical Gauge Field, Phys. Rev. Lett. **129**, 180401 (2022).

[30] M. A. Gorlach and A. N. Poddubny, Topological edge states of bound photon pairs, Phys. Rev. A **95**, 053866 (2017).

[31] G. Salerno, G. Palumbo, N. Goldman, and M. Di Liberto, Interaction-induced lattices for bound states: Designing flat bands, quantized pumps, and higher-order topological insulators for doublons, Phys. Rev. Res. **2**, 013348 (2020).

[32] A. S. Sheremet, M. I. Petrov, I. V. Iorsh, A. V. Poshakinskiy, and A. N. Poddubny, Waveguide quantum electrodynamics: Collective radiance and photon-photon correlations, arXiv:2103.06824.

[33] K. Winkler, G. Thalhammer, F. Lang, R. Grimm, J. Hecker Denschlag, A. J. Daley, A. Kantian, H. P. Büchler, and P. Zoller, Repulsively bound atom pairs in an optical lattice, Nature (London) **441**, 853 (2006).

[34] R. T. Piil, N. Nygaard, and K. Mølmer, Scattering and binding of different atomic species in a one-dimensional optical lattice, Phys. Rev. A **78**, 033611 (2008).

[35] M. Valiente, Lattice two-body problem with arbitrary finite-range interactions, Phys. Rev. A **81**, 042102 (2010).

[36] M. Valiente, Flat band of topological states bound to a mobile impurity, arXiv:1907.08215.

[37] J.-W. Rhim and B.-J. Yang, Singular flat bands, Adv. Phys.: X **6**, 1901606 (2021).

[38] I. Ulčakar and L. Vidmar, Tight-binding billiards, Phys. Rev. E **106**, 034118 (2022).

[39] D. Leykam, K. Y. Bliokh, C. Huang, Y. D. Chong, and F. Nori, Edge Modes, Degeneracies, and Topological Numbers in Non-Hermitian Systems, Phys. Rev. Lett. **118**, 040401 (2017).

[40] Z. Gong, Y. Ashida, K. Kawabata, K. Takasan, S. Higashikawa, and M. Ueda, Topological Phases of Non-Hermitian Systems, Phys. Rev. X **8**, 031079 (2018).

[41] K. Kawabata, K. Shiozaki, M. Ueda, and M. Sato, Symmetry and Topology in Non-Hermitian Physics, Phys. Rev. X **9**, 041015 (2019).

[42] H. Fukuyama, R. A. Bari, and H. C. Fogedby, Tightly bound electrons in a uniform electric field, Phys. Rev. B **8**, 5579 (1973).

[43] E. E. Mendez and G. Bastard, Wannier-Stark ladders and Bloch oscillations in superlattices, Phys. Today **46**(6), 34 (1993).

[44] M. Glück, A. R. Kolovsky, and H. J. Korsch, Wannier-Stark resonances in optical and semiconductor superlattices, Phys. Rep. **366**, 103 (2002).

[45] M. Schulz, C. A. Hooley, R. Moessner, and F. Pollmann, Stark Many-Body Localization, Phys. Rev. Lett. **122**, 040606 (2019).

[46] E. van Nieuwenburg, Y. Baum, and G. Refael, From Bloch oscillations to many-body localization in clean interacting systems, Proc. Natl. Acad. Sci. USA **116**, 9269 (2019).